


Volume 52, Issue 4, April 2010 ISSN 0010-938X



CORROSION SCIENCE

The Journal on Environmental Degradation of Materials and its Control
Editor-in-Chief: G. T. BURSTEIN, University of Cambridge, U.K.
An Official Journal of the Institute of Corrosion

CONTENTS

Letter		
P. M. KARLSSON, M. W. ANDERSON and A. E. C. PALMOVIST	1103	Adsorption of sodium dodecyl sulfate and sodium dodecyl phosphate at the surface of aluminium oxide studied with AFM
Papers		
K. N. ALLAHAR, G. P. REURWAGEN and V. J. GILLING	1106	Understanding ac-de-ac accelerated test results
G. R. ENGLEHARDT and D. D. MACDONALD	1115	Modelling the crack propagation rate for corrosion fatigue at high frequency of applied stress
Y.-H. YOO, Y.-S. CHOI, J.-G. KIM and Y.-S. PARK	1123	Effects of Ce, La and Ba addition on the electrochemical behavior of super duplex stainless steels
A. NAGAOKA, K. YOKOYAMA and J. SAKAI	1130	Evaluation of hydrogen absorption behaviour during acid etching for surface modification of commercial pure Ti, Ti-6Al-4V and Ni-Ti superelastic alloys
H. KIM and D. D. MACDONALD	1139	Measurement of steady-state hydrogen electrode reactions on Alloys 600 and 690 tubes
H. SHAIKH, T. ANITA, R. K. DAYAL and H. S. KHAYAT	1146	Effect of metallurgical variables on the stress corrosion crack growth behaviour of AISI type 316LN stainless steel
D. GONZALEZ, D. ROSENZ, P. PIGIAT and M. CONFORTI	1155	Descaling ability of low-alloy steel wires depending on composition and rolling process
X. LI, S. DING, H. FU and G. MU	1167	Synergistic inhibition effect of rare earth cerium(IV) ion and sodium oleate on the corrosion of cold rolled steel in phosphoric acid solution
A. NAGANUMA, K. FURUSHI, K. AZUMI, H. HAYAZAKI and H. KONNO	1179	Application of the multichannel electrode method to monitoring of corrosion of steel in an artificial crevice
C. L. LAI, L. W. TSAI, W. KAI and C. CHEN	1187	The effects of cold rolling and sensitisation on hydrogen embrittlement of AISI 304L welds
M. A. AMIN and K. F. KHALEED	1194	Copper corrosion inhibition in O ₂ -saturated H ₂ SO ₄ solutions
Q. HU, Y. B. QIU, X. P. GUO and J. Y. HUANG	1205	Crevice corrosion of Q235 carbon steels in a solution of NaHCO ₃ and NaCl

Contents continued on outside back matter
<http://www.elsevier.com/locate/corsci>

This article appeared in a journal published by Elsevier. The attached copy is furnished to the author for internal non-commercial research and education use, including for instruction at the authors institution and sharing with colleagues.

Other uses, including reproduction and distribution, or selling or licensing copies, or posting to personal, institutional or third party websites are prohibited.

In most cases authors are permitted to post their version of the article (e.g. in Word or Tex form) to their personal website or institutional repository. Authors requiring further information regarding Elsevier's archiving and manuscript policies are encouraged to visit:

<http://www.elsevier.com/copyright>



Contents lists available at ScienceDirect

Corrosion Science

journal homepage: www.elsevier.com/locate/corsci

Influence of oxidizing ability of the medium on the growth of lanthanide layers on galvanized steel

M. Olivier^{a,*}, A. Lanzutti^b, C. Motte^c, L. Fedrizzi^b^a Department of Materials Science, UMONS, University of Mons, Faculty of Engineering, Place du Parc 20, 7000 Mons, Belgium^b Department of Chemical Science and Technology, University of Udine, Via del Cotonificio 108, 33100 Udine, Italy^c Materia Nova Research Centre, Parc Initialis, Avenue Copernic, 7000 Mons, Belgium

ARTICLE INFO

Article history:

Received 18 September 2009

Accepted 11 January 2010

Available online 20 January 2010

Keywords:

A. Zinc

B. EIS

B. Surface analytical techniques

B. SVET

C. Oxygen reduction inhibition

ABSTRACT

Protection mechanisms offered to galvanized steel by lanthanide salts in a 0.1 M NaCl solution were investigated by using electrochemical techniques such as polarization curves, electrochemical impedance spectroscopy (EIS), scanning vibrating electrode technique (SVET) and surface analysis such as scanning electron microscope (SEM) and glow discharge optical emission spectrometry (GDOES).

The role of the oxidizing ability of the medium was studied by changing the aeration conditions: aerated, saturated, deaerated and acid deaerated solutions.

In aerated solution, the cerium deposition quickly offers an inhibition of the oxygen reduction. Current density cartographies (SVET) are consistent with surface analysis and other electrochemical techniques.

© 2010 Elsevier Ltd. All rights reserved.

1. Introduction

Chromate compounds were widely used in surface treatment industry to improve the corrosion protection of many metallic substrates such as steel, galvanized steel, aluminium and magnesium alloys. These compounds constituted the main component of acidic conversion baths for over 50 years and were also largely inserted as inhibitors in organic coatings to offer self-healing properties to metallic substrate in case of defect or failure. However, hexavalent chromium presents very high toxicity and has a bad environmental impact. For these reasons, an intense research effort was carried out to replace chromates in conversion and organic coatings by more environmentally friendly compounds for automotive, buildings, aeronautic applications and household appliances. Lanthanide compounds are reported as one of numerous alternatives for the conversion coatings [1–3]. In particular, cerium-based conversion coatings have been tested for a wide range of metals such as aluminium alloys [4–17], magnesium alloys [18–20], tin [21], zinc-plated steels [22–28] and carbon steel [29,30].

The salts showing the best performance in terms of conversion coatings and inhibitive efficiency are the cerium salts. The studied layers were mainly based on the use of cerium nitrate [10–14,26,27,30], cerium perchlorate [8,9] and cerium chloride [4,6,7,11,13,14,27,29]. Many studies concerning formation mechanisms of layers from simple rare earth salt solutions at near-neu-

tral pH [6,13,19–27] or with addition of H₂O₂ [4,5,9,11–14,29] were proposed. Without hydrogen peroxide, the dissolved oxygen is the driving force of the film formation. The reduction of dissolved oxygen occurs at the cathodic sites on the metal surface and is accompanied by simultaneous anodic dissolution of the metallic substrate. The local increase of pH resulting from the reduction of oxygen can induce precipitation of cerium hydroxides. The addition of hydrogen peroxide accelerates the film formation and induces the oxidation from Ce (III) to Ce (IV).

Despite the numerous studies, the role of species which contribute to the layer formation, kinetics of deposition, effect of the rare earth oxidation state and its concentration on the protection performance on the galvanized steel are not well understood. In this paper, the role of oxidizing ability of the medium was studied by varying the aeration conditions or the pH of the electrolytic solution. The aim of this study is not to obtain in a short time a conversion layer but to evaluate the self-healing properties of low concentration rare earth salt solutions which frequently are proposed as inhibiting species to be introduced in the nano-reservoirs of new designed environmentally friendly coatings.

Considering the corrosion of galvanized steel duplex systems, two potential failure mechanisms have to be taken into account. On one hand, a defect or damage in the organic coating may lead to direct exposure of the zinc surface to the environment and generalized corrosion may occur. On the other hand, metallic cut edges exposed when the galvanized steel sheets are cut to size are areas of particular susceptibility to galvanic corrosion.

* Corresponding author. Tel.: +32 65374431; fax: +32 65374416.

E-mail address: Marjorie.Olivier@umons.ac.be (M. Olivier).

Among the classical electrochemical techniques, potentiodynamic polarization and EIS measurements are well suited techniques to study the inhibition effect of the lanthanides inhibitors on the zinc layer corrosion of the HDG steel. The changes observed in the polarization curves give an indication of the role played by the inhibitor. Both cathodic and anodic inhibitors reduce the corrosion current, shifting negatively (cathodic inhibitor) or positively (anodic inhibitor) the corrosion potential. Although the obtained impedance spectra are often difficult to analyze for the longer immersion times, the low frequency impedance modulus values give an indication of the corrosion resistance of the system. The evolution of the time constants also gives valuable information on the corrosion mechanism.

Despite the importance of the classical electrochemical techniques, the obtained results refer to the whole area of the working electrode but do not give information on the currents distribution on the surface. In recent years, several techniques have been developed which give valuable information on the behaviour of a corroding system at a microscopic level [31–34]. The SVET technique has been successfully used for monitoring many corrosion situations [32–36]. In the present study, the efficiency of corrosion inhibition on zinc surface of HDG steel sample when a low concentration in chloride cerium is added to a sodium chloride solution is investigated by the SVET technique. The SVET technique is based on the measurement of small potential variation due to the fluxes of ionic currents originated by the electrochemical reactions that occur on the active surface. Ions are formed and distributed in solution with concentration gradients that create electric fields. These gradients can be detected by a probe vibrating over the corroding surface and can be converted in current densities using Ohm's law.

In order to obtain more information concerning the morphological structure of the cerium layers, GDOES profiles, SEM and profilometric measurements are performed on the galvanized steel after 24 h of immersion in the electrolytic solution containing the same concentration in inhibitors species but changing the oxidizing ability of the medium (dissolved oxygen concentration and pH).

2. Materials and methods

The specimens were cut from continuous hot-dip galvanized (HDG) steel sheets supplied by ArcelorMittal (≈ 0.25 wt.% Al). In this process, the HDG steels were submitted to a skin pass after cooling and galvanization. The steel width was about 0.8 mm and the thickness of the zinc coating was in the range of 7–10 μm .

Before measurements, the samples were degreased using an alkaline solution at pH = 9.5 and 60 °C (Gardoclean S5080 from Chemetall, concentration = 10 g/l) and thoroughly rinsed with deionised water. Directly after surface cleaning, the samples were immersed in chosen electrolytes. The immersed area of samples was 4.5 cm^2 .

The electrolytic solutions were prepared using analytical grade NaCl and consisted of aerated solution ([dissolved O_2] = 8 ppm by mass), saturated solution ([dissolved O_2] = 40 ppm by mass) and deaerated solution (less than 2 ppm by mass of oxygen) of 0.1 M NaCl with and without inhibitive species. The different oxygenation ratios were obtained at 23 ± 1 °C by bubbling oxygen (saturated) or nitrogen (deaerated) at low flow into the solutions or by exposition to atmospheric conditions (aerated) and evaluated by means of a Consort Z621 oximeter. The rare earth salts used as inhibitors were $\text{CeCl}_3 \cdot 7\text{H}_2\text{O}$, $\text{YCl}_3 \cdot 6\text{H}_2\text{O}$ and $\text{LaCl}_3 \cdot 7\text{H}_2\text{O}$. The salts were introduced in the electrolytic solution at a concentration of 2.5 mM. This concentration was chosen following previous results [27].

The corrosion behaviour of HDG in the different electrolytic solutions was studied by means of potentiodynamic polarization and EIS. A conventional three-electrode cell which consists of the sample as the working electrode, a platinum sheet as the counter electrode and an Ag/AgCl/KCl(sat) electrode as the reference electrode is used. All the measurements were carried out inside a Faraday cage in order to minimize external interference.

The polarization measurements were performed using a 283 EG&G potentiostat after immersion of the HDG samples in electrolytic solutions with and without inhibitor. Different specimens were employed for the potentiodynamic polarization measurements in the anodic and cathodic directions. The cathodic and anodic curves were recorded at a scan rate of 100 mV/min starting from the open circuit potential.

For EIS measurements, the M398 software is used to control the EG&G PAR 283 potentiostat connected to a 1025 frequency response analyzer. The swept frequency range varies from 100 kHz to 10 mHz. A sinusoidal signal of 5 mV (rms) in amplitude is superimposed to the open circuit potential.

All the classical electrochemical experiments were carried out at least in triplicate.

A commercial SVET system (Perkin Elmer SVP 100) from Ametek was used in this work.

Before measurement, calibration of the SVET is achieved by employing a PIS (point in space) electrode. A known current is injected into a gold wire of 100 μm radius and is correlated with the SVET output signal.

Local electrochemical measurements were carried out with the electrode vibrating at 100 μm above the surface of the sample with 30 μm of amplitude. The SVET was used in sweep scan mode with a sweep rate of 1000 $\mu\text{m}/\text{s}$. The scan area was typically 4000×3000 μm along the flat sample. The duration of a scan is approximately 20 min.

In order to maintain the same chloride concentration and conductivity, the surface of galvanized steel samples were exposed to solutions containing 2.5 mM NaCl ($\chi = 320$ $\mu\text{S}/\text{cm}$) and 1.75 mM NaCl + 0.25 mM CeCl_3 ($\chi = 292$ $\mu\text{S}/\text{cm}$). Repetitive scans were taken up to 24 h of immersion.

The GDOES analysis was carried out using a JY RF-GD PROFILER HR instrument, manufactured by Horiba Jobin-Yvon, Longjumeau, France. The instrument is equipped with a standard 4 mm diameter anode, a polychromator with 28 acquiring channels and a Quantum XP software. The source conditions, employed for the analysis, were Ar pressure of 650 Pa and 30 W applied power. These conditions are necessary to have a flat crater in order to increase the depth resolution. All results shown were obtained with the same source conditions and with the same calibration method. The calibration was performed with 30 samples selected among SUS and CRM's.

The mechanical profilometer used for analysis is a Dektak 150 manufactured by Veeco. This instrument is equipped with a stylus with tip radius of 12.5 μm . The stylus is mechanically coupled with a linear variable differential transformer and the maximum step for profile acquisition is 1 mm. Information about 3D maps and linear analysis are computed by Dektak software for data acquisition and for operating the profilometer. The Vision software is employed to elaborate and view 3D maps.

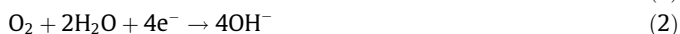
The area analyzed was 2 mm \times 1 mm with a scan resolution of 0.333 points/ μm and lateral resolution of 1 line/2 μm . A low pass filter was used to reduce abnormal spikes on surface for some pictures.

A Philips XL 20 scanning electron microscope equipped with an EDAX energy dispersive X-ray spectrometer was used. For SEM observations and EDX analysis, flat samples of HDG steel (before and after inhibitive treatment) were used.

3. Results

3.1. Classical electrochemical techniques

The kinetic effect of the different compounds on the generalized corrosion of HDG steel is investigated by recording polarization curves and impedance spectra after different immersion times. Corrosion of zinc in a near neutral oxygenated solution occurs by combination of the zinc anodic dissolution (1) and the cathodic oxygen reduction (2):



Because of the low solubility of zinc hydroxide ($K_s[\text{Zn}(\text{OH})_2] = 3 \times 10^{-17}$), the HDG steel samples are probably initially covered with an (hydr)oxide layer which offers a slight protection to the generalized corrosion of zinc. In presence of chloride, this layer evolves to form soluble hydroxychloride complexes allowing corrosion onset.

The presence of an inhibitor can produce a potential shift towards more positive values indicating a decrease of the oxidation rate. On the other hand, a negative potential shift means that the cathodic reaction is inhibited. The measurement of the mixed potential with immersion time in the different electrolyte solutions is shown in Fig. 1 and is useful to determine the time needed to obtain a stabilized system before polarization curve measurements.

After 2 h of immersion in aerated solution, the values of mixed electrode potential, for each solution containing an inhibitor, is almost stable. Yttrium chloride showed a cathodic inhibition effect with a marked decrease of OCP value compared to the value obtained without inhibitor. Cerium and lanthanum salts do not induce a shift of the OCP value. This behaviour can be explained by a simultaneous decrease of the cathodic reaction rate and the formation of a rare earth oxide layer.

Fig. 2a shows the anodic and cathodic polarization curves obtained for each inhibitor after 2 h of immersion in the aerated electrolyte solution containing the inhibitor. An important decrease of the oxygen reduction rate can be observed on the cathodic side. This behaviour is mainly marked for lanthanum. In anodic polarization curves, a small inflection of the curves for small overvoltage can be detected in presence of each inhibitor. This inflection is slightly more pronounced for yttrium, even though its anodic current density is higher. However, a significant decrease of the corrosion current due to the inhibitor efficiency after a short

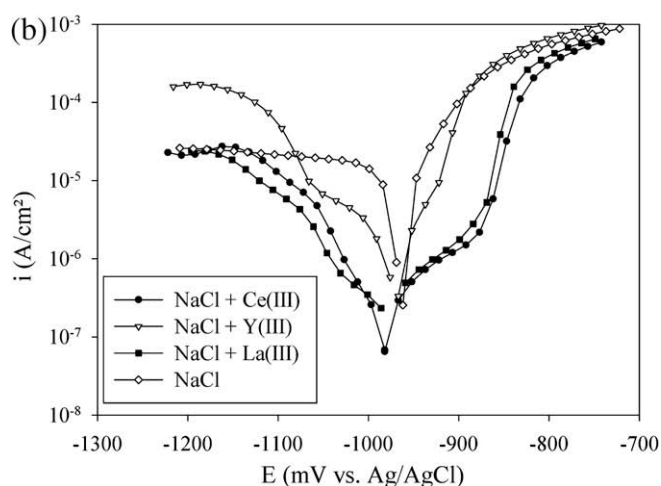
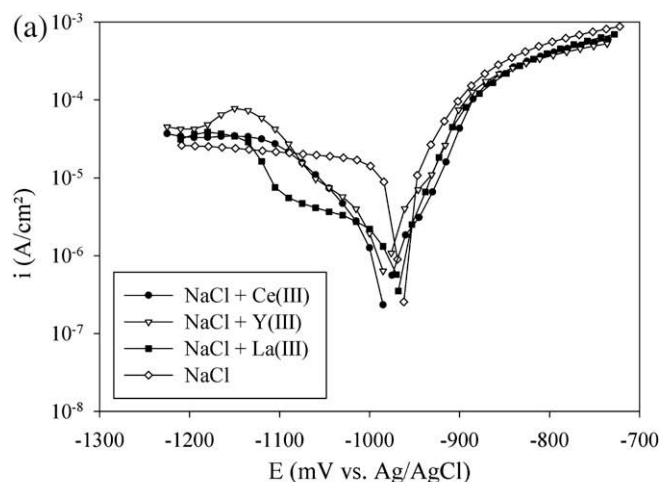
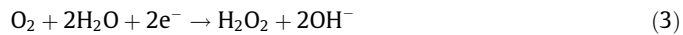


Fig. 2. Anodic and cathodic polarization curves of HDG samples in 0.1 M NaCl solution without inhibitor, with 2.5 mM CeCl₃, 2.5 mM YCl₃ and 2.5 mM LaCl₃ after 2 h (a) and 24 h (b) of immersion.

immersion time can be mentioned for each compound in aerated medium.

After 24 h of immersion in aerated medium (Fig. 2b), oxygen reduction is even more inhibited for each inhibitor (apart from yttrium) and more clearly presents two reduction waves. The oxygen reduction seems to occur in two steps:



The first wave could correspond to the formation of hydrogen peroxide [28,29].

The anodic inhibition is clearly visible for lanthanum and cerium salts with apparition of a large passivity range (about 130 mV) probably due to the precipitation of a homogeneous protective oxide layer. The corrosion current decreases significantly with immersion time for each inhibitor. The lowest value of the corrosion current was obtained for the cerium. For this reason, this inhibitor was chosen to study the influence of the oxidizing ability of the medium on formation of the protective layers.

In order to evaluate the protective performances with immersion time and the oxidizing ability of medium, HDG samples were immersed in aerated solution ([dissolved O₂] = 8 ppm by mass), saturated solution ([dissolved O₂] = 40 ppm by mass) and deaerated solution (less than 2 ppm by mass of oxygen) with 0.1 M NaCl and 2.5 mM CeCl₃, respectively. After different immersion times,

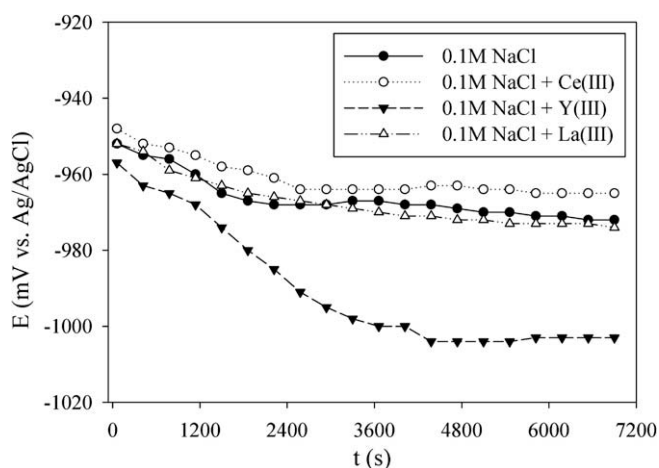


Fig. 1. Mixed potential versus time in 0.1 M NaCl solution without inhibitor, with 2.5 mM CeCl₃, 2.5 mM YCl₃ and 2.5 mM LaCl₃.

the samples were analyzed by electrochemical impedance measurement in 0.1 M NaCl aerated electrolyte with or without inhibitor.

The low frequency impedance modulus values obtained at 0.01 Hz ($|Z|_{0.01 \text{ Hz}}$) can be used to estimate the total resistance of the system and can be considered as an approximation of the reverse of its corrosion rate.

In the aerated solution, after 1 h of immersion, the Bode-modulus diagrams (Fig. 3) show a markedly increase of the corrosion resistance of the system in presence of cerium chloride since the $|Z|_{0.01 \text{ Hz}}$ values are increased by more than one order of magnitude ($29.05 \text{ k}\Omega \text{ cm}^2$) compared to the HDG in sodium chloride solution without any inhibitor ($0.95 \text{ k}\Omega \text{ cm}^2$). The spectrum obtained for bare HDG samples is complex due to the different phenomena occurring at the metal/solution interface such as corrosion and porous corrosion products formation. For the samples immersed in the electrolyte containing the lanthanide inhibitor, after 24 h of immersion only one time constant, present in a large range of frequencies is clearly visible which may be attributed to the formation of a protective layer at the HDG steel surface.

For longer exposure times, low frequency impedance modulus value progressively increases and after 1 day, the $|Z|_{0.01 \text{ Hz}}$ obtained on the HDG samples reaches a magnitude order of $110 \text{ k}\Omega \text{ cm}^2$. At

the end of the test the surface of the HDG steels samples showed no sign of corrosion activity. These results are in good agreement with the polarization curves obtained for the same immersion time.

In order to evaluate the layer performance, the HDG steel samples were immersed during different times in the inhibitive solutions having different aeration conditions and analyzed by EIS after these times in the inhibitive aerated aggressive solution. For the samples immersed in the inhibitive oxygen saturated solution (Fig. 4) for 1 h the low frequencies modulus ($|Z|_{0.01 \text{ Hz}}$) increases and reaches $7.1 \text{ k}\Omega \text{ cm}^2$ compared to $16.6 \text{ k}\Omega \text{ cm}^2$ for the samples immersed in an aerated solution.

The $|Z|_{0.01 \text{ Hz}}$ significantly increases after the first hour of immersion due to the film formation. Nevertheless, the curve obtained for samples immersed for 6 h in saturated oxygen solutions shows a completely different behaviour either in magnitude or in phase and reveals diffusion control. After 6 h of immersion, the presence of a thick, yellow coloured and non homogeneous oxide layer is observed.

Corrosion morphology observation of this type of samples frequently evidences the formation of pits which were analyzed by SEM element mapping (Fig. 5). Cerium oxide compounds are mainly located around the pit (Fig. 5c) under large crystals form

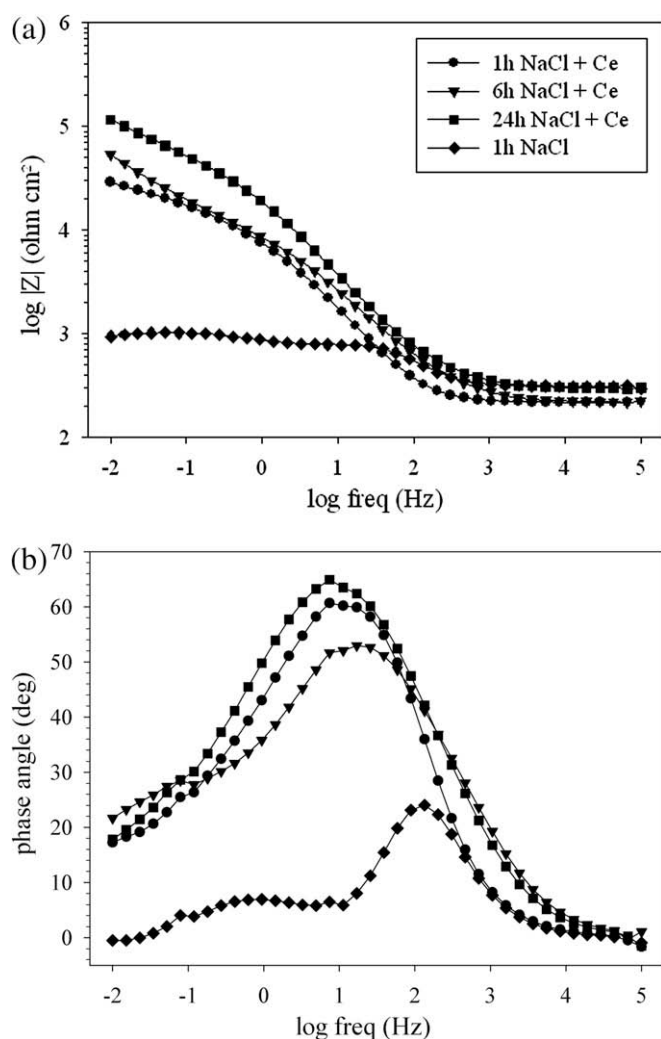


Fig. 3. Bode's diagrams in modulus (a) and phase (b) obtained for HDG samples immersed in an aerated 0.1 M NaCl solution after 1 h and aerated 0.1 M NaCl + 2.5 mM CeCl_3 after 1 h, 6 h and 24 h, respectively. The electrolyte used for the measurement is the electrolyte used during immersion.

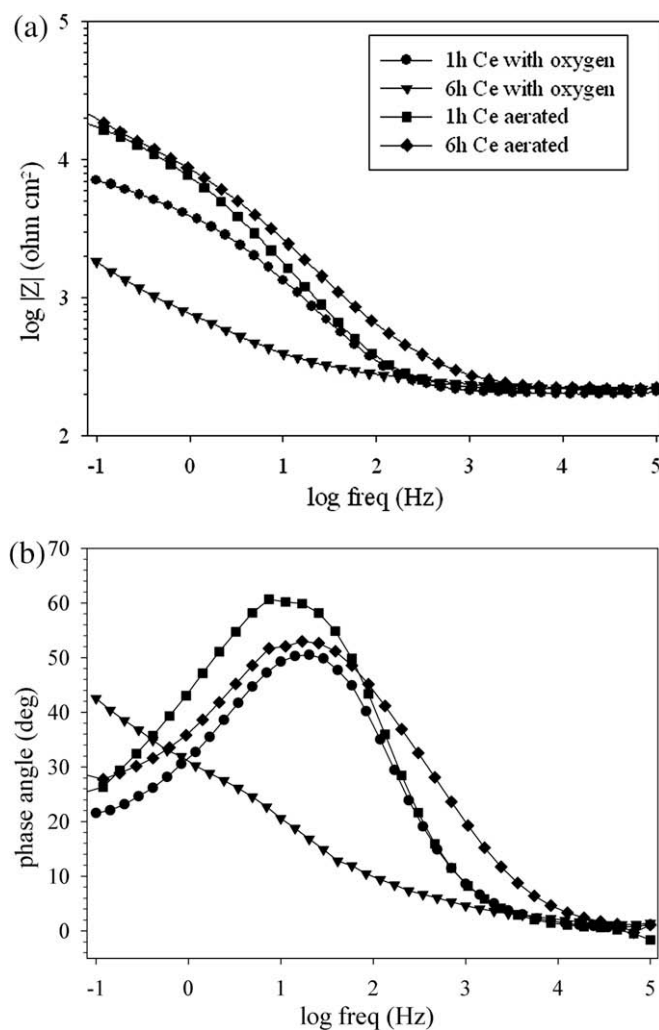


Fig. 4. Bode's diagrams in modulus (a) and phase (b) obtained for HDG samples immersed in an aerated 0.1 M NaCl + 2.5 mM CeCl_3 solution after 1 h and 6 h, and in an oxygen saturated 0.1 M NaCl + 2.5 mM CeCl_3 solution after 1 h and 6 h. The electrolyte used for measurement is an aerated 0.1 M NaCl solution with inhibitor.

but also inside the pit. Moreover, after 6 h of immersion, the pits reach the steel substrate (Fig. 5d).

Probably during the first hours of immersion, cerium oxides are deposited on whole zinc surface due to the production of hydroxides ions coming from the oxygen reduction all over the surface. Due to formation of a thick, porous and heterogeneous layer, some localized anodic areas can be formed accelerating the cerium deposition around the pit corresponding to most active cathodic region. When pits reach the steel substrate, zinc becomes anode and steel is the cathode. This new galvanic cell inverses the polarities and provokes the cerium oxides deposition in the pit too.

In the deaerated solution (Fig. 6), a slight increase of the $|Z|_{0.1 \text{ Hz}}$, with respect to the not inhibited solution, can be observed ($5.6 \text{ k}\Omega \text{ cm}^2$) after 1 h of immersion and no improvement can be seen after 6 h. These values are significantly lower than those obtained after immersion in an aerated solution in the same operating conditions. This behaviour may be explained by a too low oxygen concentration which does not allow the formation of an

efficient protective layer during immersion. These results are confirmed by the presence of a second time constant in the Bode phase spectra. The time constant at low frequencies is usually associated to the corrosion process at the metal/solution interface after contact with an aerated aggressive solution.

3.2. Surface analysis

In order to obtain more information concerning the effect of the oxidizing power of the medium on cerium film formation, surface topography and GDOES profiles were performed on the bare HDG sample and on the HDG samples immersed for 24 h in an aerated solution, in an oxygen saturated one and in a deaerated solution (at $\text{pH} = 6$ and $\text{pH} = 4$) containing 0.1 M NaCl with 2.5 mM CeCl_3 .

The surface topography of the bare skin passed HDG sample is clearly observed by using profilometry (Fig. 7). The sample showed the regular structure produced by a skin pass process, with

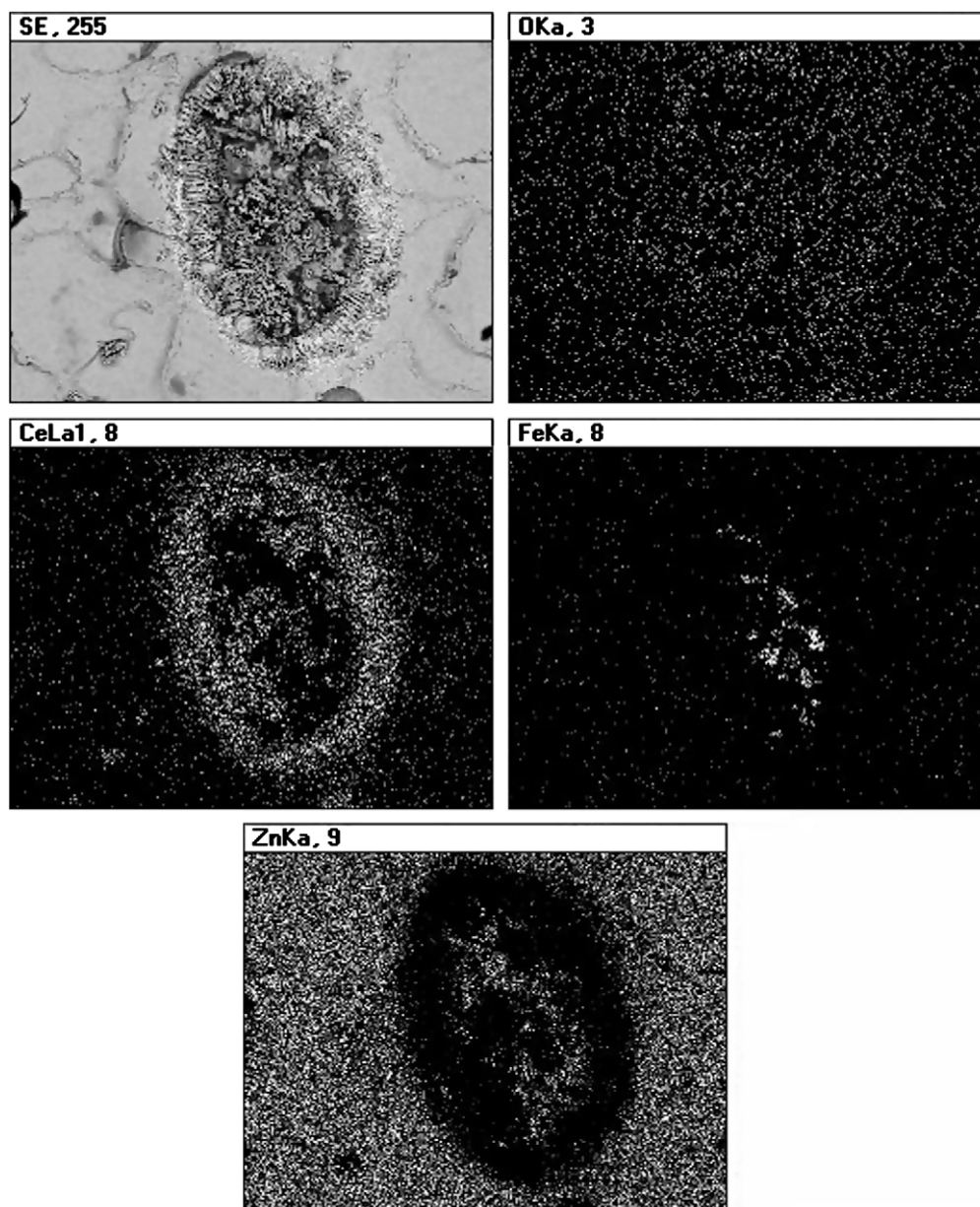


Fig. 5. SEM element mapping on a sample immersed in saturated oxygen solution containing cerium salt after 6 h of immersion.

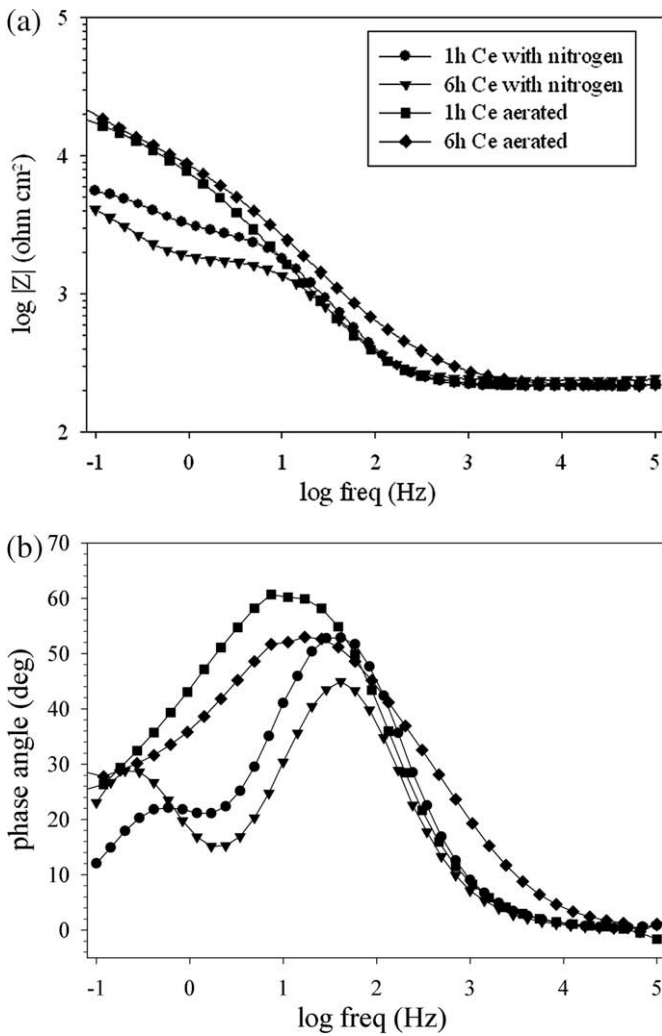


Fig. 6. Bode's diagrams in modulus (a) and phase (b) obtained for HDG samples immersed in an aerated 0.1 M NaCl + 2.5 mM CeCl₃ solution after 1 h and 6 h, and in a deaerated 0.1 M NaCl + 2.5 mM CeCl₃ solution after 1 h and 6 h. The electrolyte used for measurement is an aerated 0.1 M NaCl solution with inhibitor.

hollowed areas surrounding the protruding ones. The mean roughness of the sample is about 6 μm .

After immersion under aerated conditions, the optical observation reveals the presence of an almost homogeneous light blue and yellow pigmentation on the whole area; moreover the skin pass morphology of the zinc surface is still clearly visible after surface topography measurements (Fig. 8a).

The GDOES profiles (Fig. 8b) show that zinc alloy thickness is in the range of 7–10 μm with the presence of a very large zinc-iron inter-diffused layer. Only the upper part of the coating (about 3 μm) is composed by almost pure zinc (η phase). Moreover, high cerium and oxygen concentrations are evident at the top of the surface (about 30–35% and 60%, respectively). The cerium concentration remains higher than 1% up to 0.65 μm , whereas an important increase of the zinc concentration is only observed after 0.15 μm . Although the sample surface is quite rough, the sharp peak of the cerium signal on top surface reveals that this layer is homogeneously distributed on the skin-passed morphology.

After immersion in the inhibitive oxygen saturated solution, the optical observation shows a dark yellow–orange cerium deposit which seems to be thick, heterogeneous and mainly deposited in the hollowed areas. This is confirmed by the surface topography measurements (Fig. 9a) which reveal that the skin pass treatment structure is almost disappeared.

GDOES profiles (Fig. 9b) collected on these samples are highly disturbed by the lateral heterogeneous composition of the surface which is composed by cerium, oxygen and zinc. The cerium layer seems to be very thick, nevertheless, due to zinc corrosion; the top of the layer also contains zinc and oxygen up to 0.04 μm . Later on, the zinc concentration decreases (from 70% to 40%) and an increase of the cerium (6%) and oxygen is observed. For deeper erosion, the zinc concentration increases again but the cerium signal is detected in the wide depth range (8 μm). The zinc attack in this inhibitive solution seems to be important due to the high oxygen concentration and the porosity and defective structure of the cerium layer. The remarkable zinc dissolution is even confirmed by the iron signal which can be detected already after 2 μm depth suggesting a strong dissolution of the η phase.

When the HDG sample is immersed in the deaerated solution containing the cerium salt (at pH = 6), a slight iridescence appears but not exactly the typical yellow colour of the Ce (IV) hydroxides.

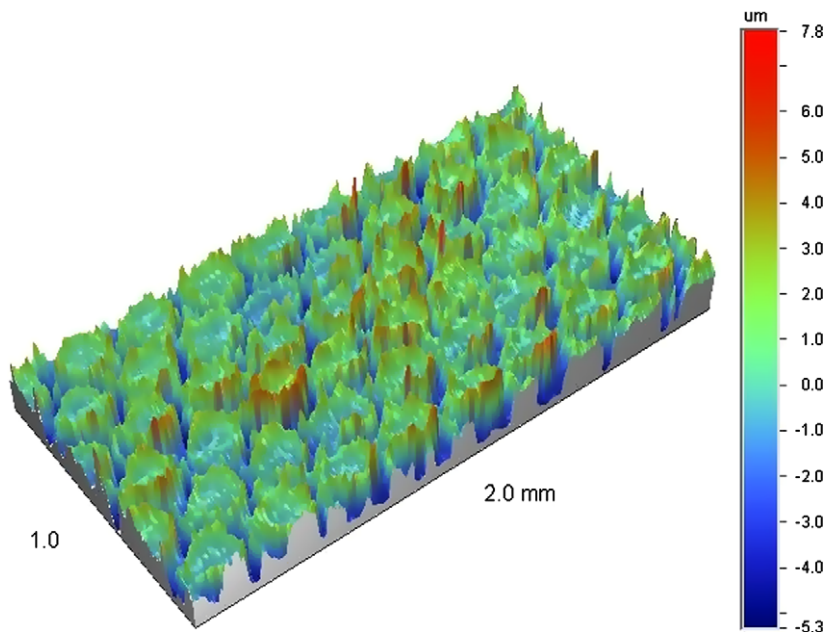


Fig. 7. Profilometry measurement of bare skin passed HDG sample.

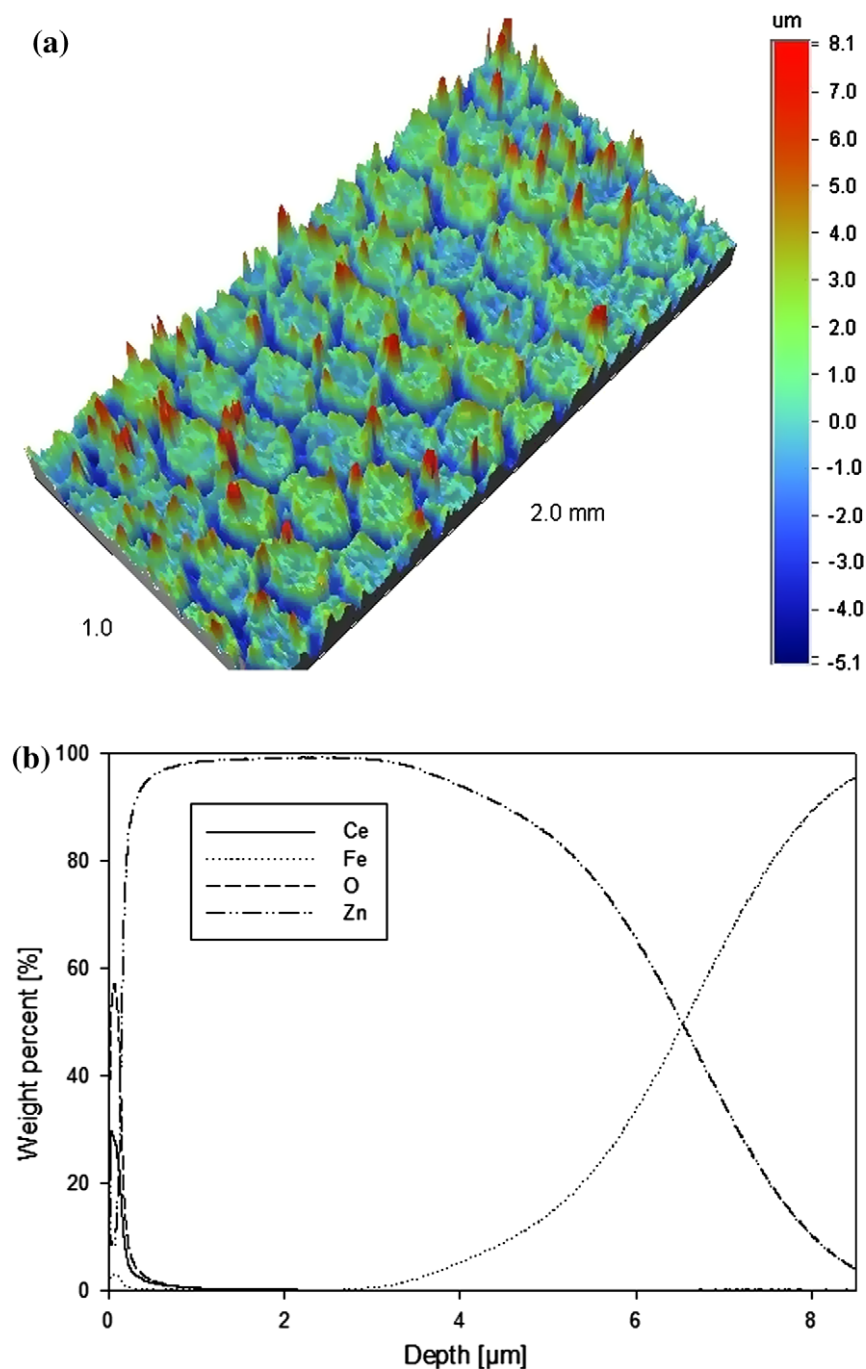


Fig. 8. Profilometry measurement (a), GDOES profiles (b) of a sample immersed for 24 h in the inhibitive aerated solution.

The skin pass surface morphology is still clearly evident (Fig. 10a), but surface topography suggests the presence of a mild surface attack of the upper zinc areas.

GDOES profiles are very similar to those acquired on samples immersed in the aerated solution and reveal that a very thin, homogeneous and reproducible layer is formed (Fig. 10b). Cerium concentration of the surface is 30% with a high presence of oxygen (50%). The zinc concentration is less than 1% at 0.03 μm but strongly increases from this depth. The layer is probably formed by cerium hydroxides produced by the water reduction.

In order to compare the different aeration conditions the results are presented in terms of the cerium/zinc ratio calculated on the whole zinc layer after 24 h of immersion in each inhibitive solutions (Fig. 11).

The highest value is obtained for the oxygen saturated one due to the important cerium hydroxides deposition induced by the important local pH increase but also due to the strong zinc dissolution. In the aerated solution, the cerium deposition is also very important but the uniform layer deposition allows avoiding significant zinc dissolution. In nitrogen saturated medium, the water reduction induces the formation of a uniform but very thin inhibitive layer at pH = 6. In the same immersion conditions but at pH = 4, the cerium layer is still much thinner. Under these conditions, the local increase of pH due to protons reduction is probably not sufficient to allow the cerium hydroxide precipitation. These results confirm that oxygen concentration is the most important driving force to induce the formation of a protective cerium layer.

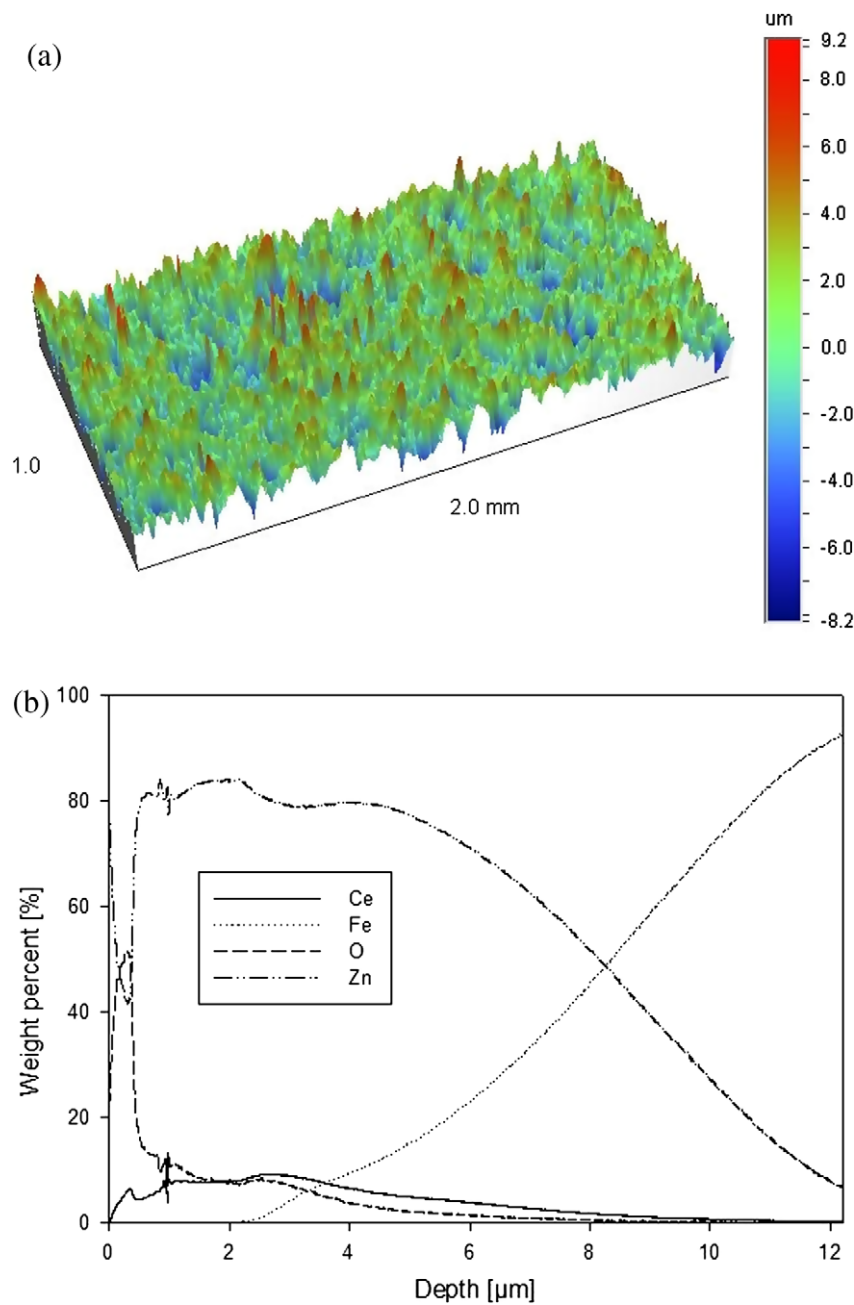


Fig. 9. Profilometry measurement (a) and GDOES profiles (b) of a sample immersed for 24 h in the inhibitive oxygen saturated solution.

3.3. SVET measurements

The investigation of the corrosion inhibition properties offered by the cerium chloride in diluted NaCl solution was carried out on the zinc surface of HDG samples. The electrolyte solution employed was an aerated one where the cerium salt exhibited the highest inhibition efficiency. This method is an electrochemical mapping technique that resolves and quantifies localized corrosion. It was used to investigate pitting and corrosion phenomena like corrosion at cut edges and zinc dissolution [35,36]. These measurements were performed using a more diluted concentration of the inhibitor with respect to the previous tests.

On the zinc surface of the HDG steel sample, two kinds of experiments were carried out. In the first one, the sample was put in contact with the aggressive sodium chloride solution and scanned for 1 h 30 min. After this time, the electrolyte solu-

tion was replaced by a solution having the same conductivity but containing cerium salt. In the second experiment, the sample was directly immersed in the solution containing the cerium salt.

The SVET maps were obtained periodically during immersion in solution as depicted in Fig. 12. In sodium chloride solution without any inhibitor, the pitting corrosion of the zinc surface is already visible after 30 min of immersion (anodic activity corresponding to a current density of $200 \mu\text{A}/\text{cm}^2$) and becomes more active with immersion time ($400 \mu\text{A}/\text{cm}^2$ and $800 \mu\text{A}/\text{cm}^2$ after 60 and 90 min, respectively). After replacement of the sodium chloride solution by the solution containing cerium chloride, the anodic activity significantly decreases and localized corrosion seems to disappear. Nevertheless, a pitting attack appears again after 2 h. Due to the low concentration of cerium and the intense initial anodic activity is not able to completely inhibit a pitting corrosion.

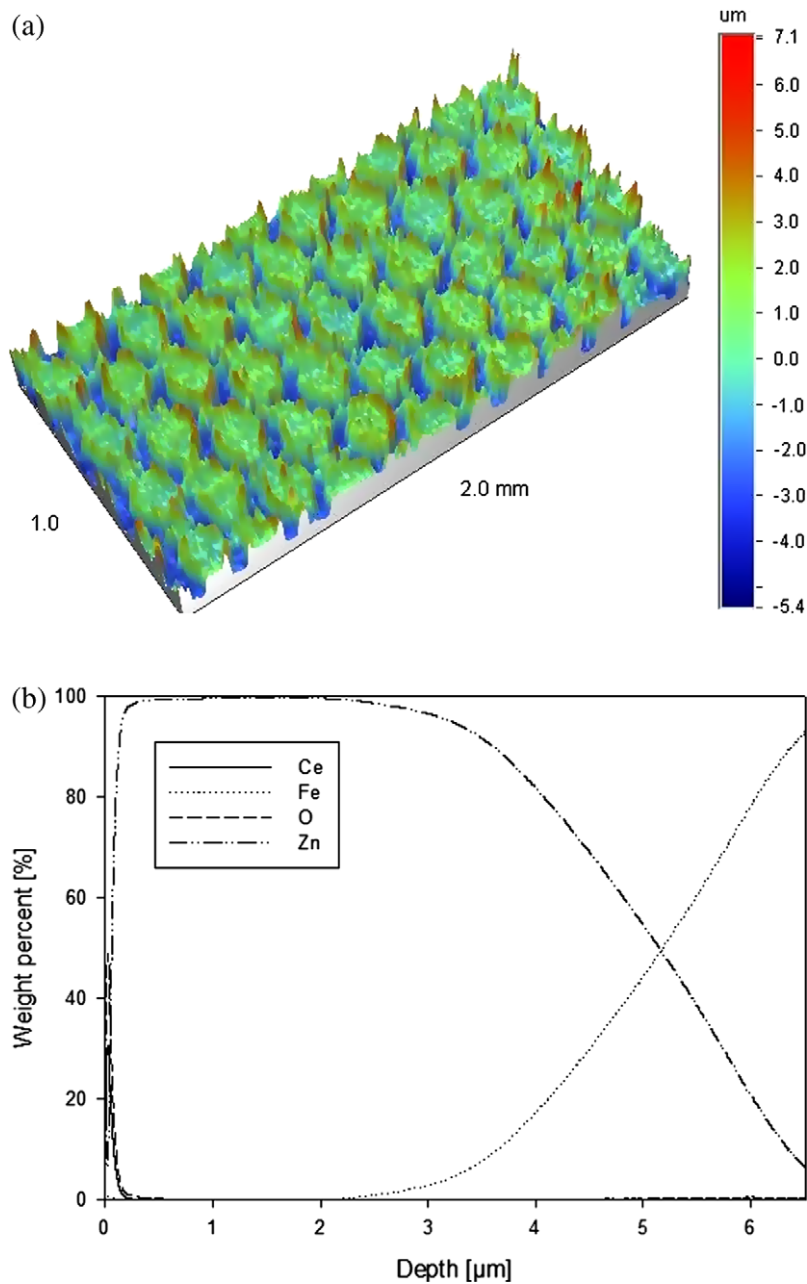


Fig. 10. Profilometry measurement (a) and GDOES profiles (b) of a sample immersed for 24 h in the inhibitive deaerated solution at pH = 6.

For the second experiment, when the sample is directly put in contact with the solution containing cerium salt, the maps do not show development of anodic and cathodic activities even after 6 h of immersion (Fig. 13). This result means that either uniform corrosion is present on the zinc surface or the efficiency of cerium salts allows the formation of a protective layer preventing corrosion phenomenon and pitting corrosion. After 6 h of immersion, no white rust was observed on the surface which showed the typical light-yellow colour of the cerium hydroxides present on whole surface. These results seem to confirm the good efficiency of the cerium salts in aerated solution.

4. Discussion

From a thermodynamical point of view [37], the formation of the trivalent cerium hydroxides from an aqueous solution contain-

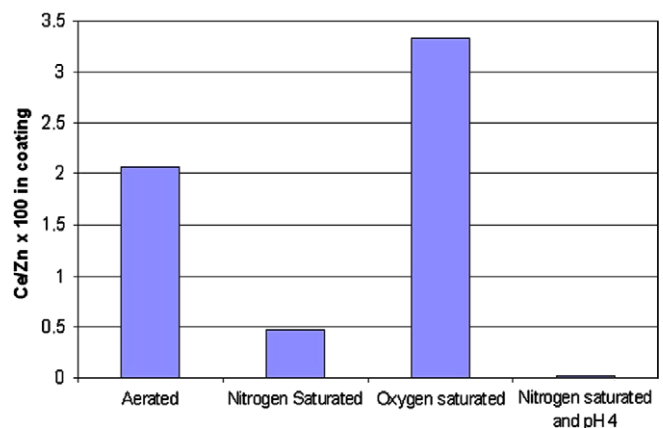


Fig. 11. Comparison of the different aeration conditions in terms of cerium/zinc ratio.

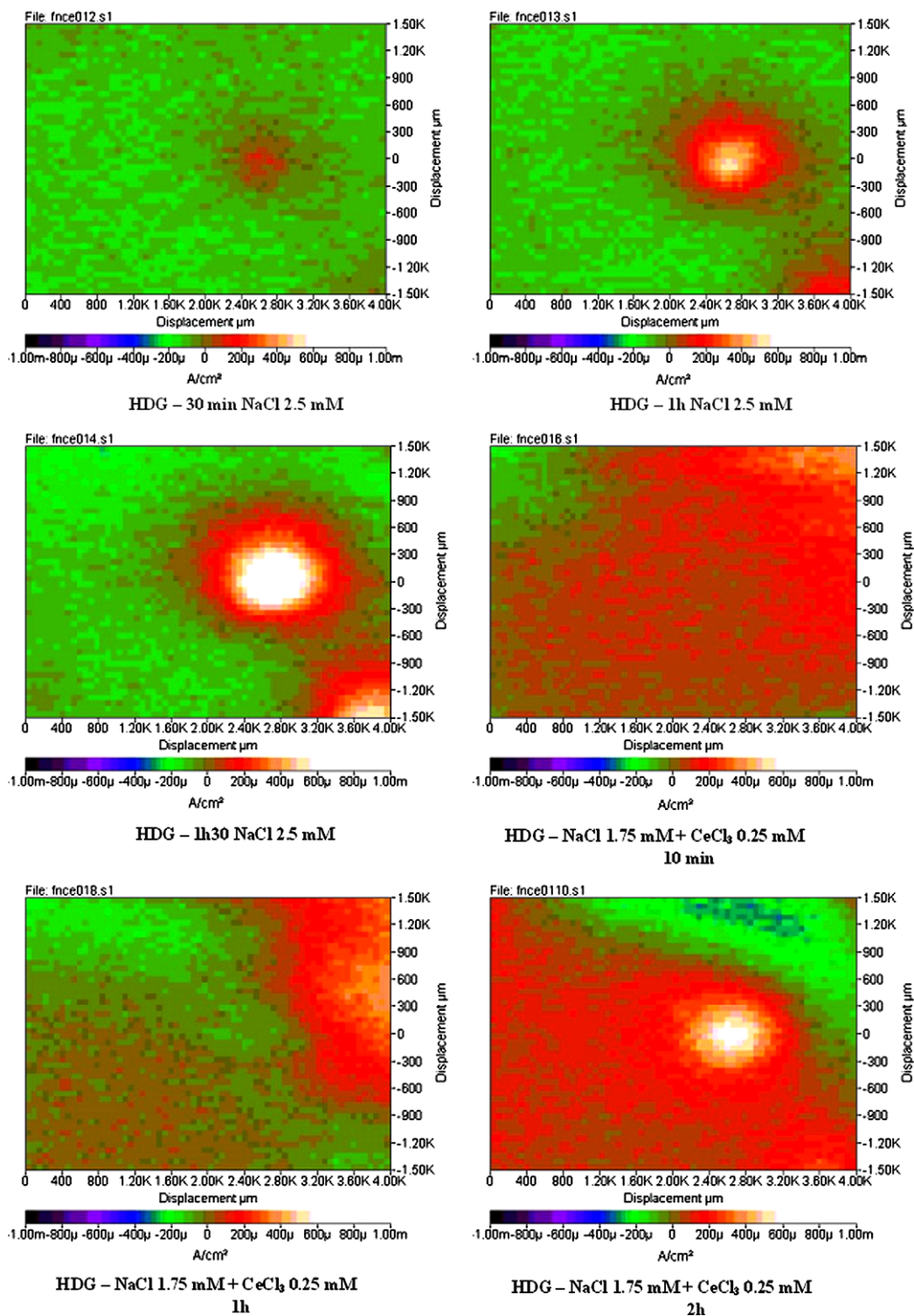
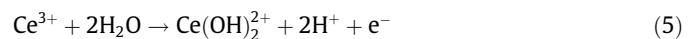


Fig. 12. SVET mapping of the HDG steel surface after different immersion times in NaCl 2.5×10^{-4} M. The initial solution was removed by NaCl 1.75 mM + CeCl₃ 0.25 mM after 90 min.

ing the trivalent salt is only depending on the pH. For a 2.5 mM CeCl₃, this pH is about 8.25 if all cerium ions in solution are hydrolyzed. Without any convection, it was shown by Arenas et al. [28] that the local pH can reach values between 10.39 and 10.6 following the number of exchanged electrons by the cathodic reaction and thus, this value is sufficient to allow the formation of trivalent hydroxide cerium layer. The formation of a layer containing tetravalent cerium oxides is due to oxidation from Ce (III) to Ce (IV) and

a pH reaching the critical value for precipitation of the corresponding oxide.

The respective reactions are given by [17]:



The values of the redox potential and solubility are described by:

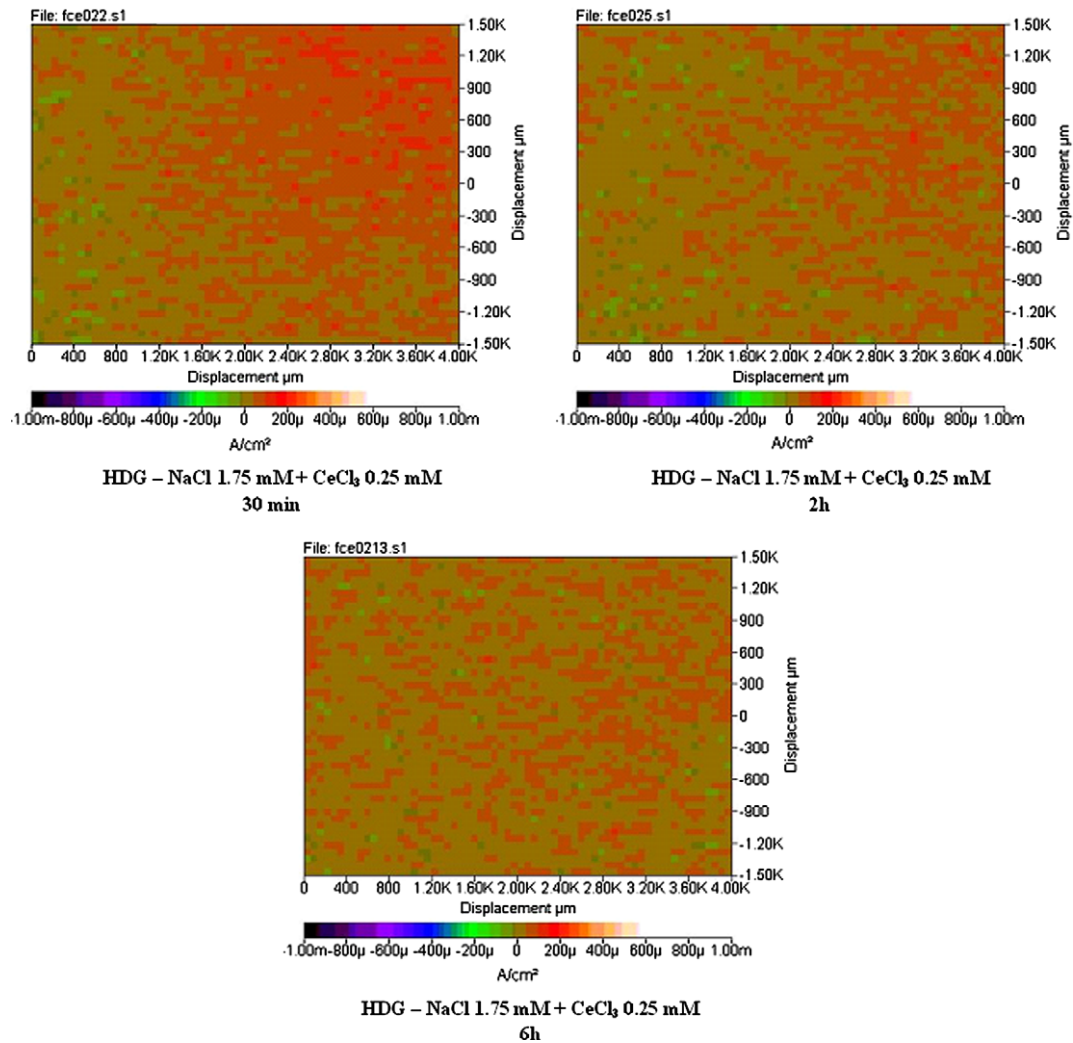


Fig. 13. SVET mapping of the HDG steel surface after different immersion times in NaCl 1.75 mM + CeCl₃ 0.25 mM.

$$E^0 = 1.731 - 0.1182\text{pH} + 0.0591 \log \left(\frac{[\text{Ce}(\text{OH})_2^{2+}]}{[\text{Ce}^{3+}]} \right) \quad (7)$$

$$\log[\text{Ce}(\text{OH})_2^{2+}] = 19.22 - 2\text{pH} \quad (8)$$

These potential and pH values will only be reached if the oxidizing power of the medium and the pH are high. In a deaerated medium whatever the pH, these conditions are not reached and the hydroxide layer contains only trivalent cerium hydroxides. When the initial pH of the deaerated medium is low, the zinc is oxidized and the protons are reduced. This reduction induces a local increase of pH and the trivalent cerium hydroxide layer is only formed if the local pH value can reach 8.25. This condition cannot be easily respected for an initial pH of 4. In that case, the layer is very thin and not protective enough.

In an aerated medium, the main cathodic reaction is the oxygen reduction which is depending on the nature of the zinc surface. As shown in the cathodic polarization curves (Fig. 2), without inhibitive species the oxygen reaction corresponds to the transfer of four electrons respecting Eq. (2). With the increase of immersion time in an aerated solution containing the trivalent cerium salt, the modification of the zinc surface induces a change in kinetics of oxygen reduction. Two reduction waves become clearly visible and can be attributed to reactions (3) and (4). The first reaction allows the formation of hydrogen peroxide whose oxidizing ability is high and able to oxidize a part of trivalent cerium [17,28,29].

$$E^0 = 1.776 - 0.0591\text{pH} + 0.0295 \log[\text{H}_2\text{O}_2] \quad (9)$$

In this medium, the layer is passivating, deposited on whole surface and composed of a mixture of Ce (III)/Ce (IV) oxides and hydroxides as shown by classical electrochemical, SVET and surface analysis.

In the oxygen saturated medium, the layer becomes thicker, orange due to the high concentration in Ce (IV) and is heterogeneous. The higher oxygen concentration facilitates the oxidation of cerium, formation of hydrogen peroxide and pH increase. Nevertheless, the corrosion products formed are more porous, not protective and cannot avoid the zinc oxidation and the apparition of pits reaching the steel substrate. The layer consists of a mixture of zinc and cerium (III)/(IV) hydroxides.

5. Conclusion

The inhibition offered by different lanthanide compounds and the influence of the oxidizing ability of the medium were studied in a sodium chloride solution.

In agreement with some previous studies, the best performance is obtained for the cerium salts in an aerated solution. In these conditions, the cerium deposition quickly offers an inhibition of the oxygen reduction. After a longer immersion time, an anodic inhibition is also clearly observed. A thin and transparent cerium layer is formed and induces a passive behaviour to the galvanized steel

substrate. The results obtained by polarization curves and EIS measurements confirm this protective behaviour.

When the solution is saturated in oxygen, the cerium layer is heterogeneous, partially yellow Ce (IV) and locally pitted. A huge amount of cerium compounds around the pits is detected confirming an easier precipitation of cerium in cathodic areas. When the pits reach the steel, the local cathodic area becomes anodic and the steel substrate becomes the main cathode allowing cerium precipitation in these areas.

The best inhibitive efficiency of the cerium layer on galvanized steel is obtained in aerated medium where the main cathodic reaction is the oxygen reduction which is limited by diffusion transport with a low oxidation ratio from Ce (III) to Ce (IV) and in absence of intense galvanic couple which facilitates the formation of porous but not protective deposits on the cathodic areas.

Acknowledgements

The authors would like to thank Nicola Stella for the results obtained during Socrates Erasmus Exchange Program between University of Udine (Italy) and the University of Mons (Belgium). This study was also done in the framework of the Opti²mat “Programme Excellence” financed by the Walloon Region (Belgium).

References

- [1] S.M. Cohen, *Corrosion* 51 (1995) 71–78.
- [2] R.G. Buchheit, A.E. Hughes, *Corrosion: Fundamentals, Testing and Protection*, vol. 13A, American Society for Materials, Materials Park, OH, 2003.
- [3] A. Nylund, *Aluminium Trans.* 2 (2000) 123.
- [4] A.E. Hughes, S.G. Hardin, T.G. Harvey, T. Nikpour, B.R.W. Hinton, A. Galassi, G. McAdam, A. Stonham, S.J. Harris, S. Church, C. Figgures, D. Dixon, C. Bowden, P. Morgan, S.K. Toh, D. McCulloch, J. Du Plessis, *ATB Metall.* 43 (2003) 264.
- [5] W.G. Fahrenholtz, M.J. O'Keefe, H. Zhou, J.T. Grant, *Surf. Coat. Technol.* 155 (2002) 208–213.
- [6] D.R. Arnott, N.E. Ryan, B.R.W. Hinton, B.A. Sexton, A.E. Hughes, *Appl. Surf. Sci.* 22–23 (1985) 236.
- [7] A.E. Hughes, J.D. Gorman, P.R. Miller, B.A. Sexton, P.J.K. Paterson, R.J. Taylor, *Surf. Interf. Anal.* 36 (2004) 290–303.
- [8] S.A. Hayes, P. Yu, T.J. O'Keefe, M.J. O'Keefe, J.O. Stoffer, *J. Electrochem. Soc.* 149 (2002) C623–C630.
- [9] B.E. Rivera, B.Y. Johnson, M.J. O'Keefe, W.G. Fahrenholtz, *Surf. Coat. Technol.* 176 (2004) 349–356.
- [10] M. Bethencourt, F.J. Botana, M.J. Cano, R.M. Osuna, M. Marcos, *Mater. Corros.* 54 (2003) 77–83.
- [11] M. Dabala, E. Ramous, M. Magrini, *Mater. Corros.* 55 (2004) 381–386.
- [12] Y. Xingwen, C. Chunan, Y. Zhiming, Z. Derui, Y. Zhongda, *Corros. Sci.* 43 (2001) 1283–1294.
- [13] M. Dabala, L. Armelao, A. Buchberger, I. Calliari, *Appl. Surf. Sci.* 172 (2001) 312–322.
- [14] C. Wang, F. Jiang, F. Wang, *Corrosion* 60 (2004) 237–243.
- [15] L.M. Palomina, P.H. Suegama, I.V. Aoki, M.F. Montemor, H.G. De Melo, *Corros. Sci.* 50 (2008) 1258–1266.
- [16] M.L. Zheludkevich, R. Serra, M.F. Montemor, K.A. Yasakau, I.M.M. Salvado, M.G. S. Ferreira, *Electrochem. Acta* 51 (2005) 208–217.
- [17] A.J. Aldykiewicz, A.J. Davenport, H.S. Isaacs, *J. Electrochem. Soc.* 143 (1) (1996) 147–154.
- [18] K. Brunelli, M. Dabala, I. Calliari, M. Magrini, *Corros. Sci.* 47 (2005) 989–1000.
- [19] H. Ardelean, C. Fiaud, P. Marcus, *Mater. Corros.* 52 (2001) 889–895.
- [20] M.F. Montemor, A.M. Simoës, M.J. Carmezin, *Appl. Surf. Sci.* 253 (2007) 6922–6931.
- [21] N. Mora, E. Cano, J.L. Polo, J.M. Puente, J.M. Bastidas, *Corros. Sci.* 46 (2004) 563–578.
- [22] S. Böhm, R. Greef, H.N. McMurray, S.M. Powell, D.A. Worsley, *J. Electrochem. Soc.* 147 (2000) 3286–3293.
- [23] K. Aramaki, *Corros. Sci.* 46 (2004) 1565–1579.
- [24] M.G.S. Ferreira, R.G. Duarte, M.F. Montemor, A.M.P. Simoës, *Electrochim. Acta* 49 (2004) 2927–2935.
- [25] M.F. Montemor, A.M. Simoës, M.G.S. Ferreira, *Prog. Org. Coat.* 44 (2002) 111–120.
- [26] M.F. Montemor, A.M. Simoës, M.G.S. Ferreira, *Prog. Org. Coat.* 43 (2001) 274–281.
- [27] C. Motte, N. Maury, M.-G. Olivier, J.-P. Petitjean, J.-F. Willem, *Surf. Coat. Technol.* 200 (2005) 2368–2375.
- [28] M. Arenas, J.J. de Damborenea, *Electrochim. Acta* 48 (2003) 3693–3698.
- [29] F.H. Scholes, S. Soste, A.E. Hughes, S.G. Hardin, P.R. Curtis, *Appl. Surf. Sci.* 253 (2006) 1170–1780.
- [30] Y. Hamlaoui, F. Pedraza, C. Remazeilles, S. Cohendoz, C. Rébéré, L. Tifouti, J. Creus, *Mater. Chem. Phys.* 113 (2009) 650–657.
- [31] F. Andreatta, M.M. Lohrengel, H. Terryn, J.H.W. de Wit, *Electrochim. Acta* 48 (2003) 3239–3247.
- [32] A.M. Simoës, J. Torres, R. Picciochi, J.C.S. Fernandes, *Electrochim. Acta* 54 (2009) 3857–3865.
- [33] R.M. Souto, Y. Gonzalez-Garcia, A.C. Bastos, A.M. Simoës, *Corros. Sci.* 49 (2007) 4568–4580.
- [34] J. Elvins, J.A. Spittle, H. Sullivan, D. Worsley, *Corros. Sci.* 50 (2008) 1650–1658.
- [35] V. Vignal, H. Krawiec, O. Heintz, R. Oltra, *Electrochim. Acta* 52 (2007) 4994–5001.
- [36] K. Ogle, S. Morel, D. Jacquet, *J. Electrochem. Soc.* 153 (2006) B1–B5.
- [37] M. Pourbaix, *Atlas of Electrochemical Equilibria in Aqueous Solutions*, NACE, Houston, TX, 1974. p. 187.